- 1 Iron "Ore" Nothing: Benthic iron fluxes from the oxygen-deficient Santa Barbara Basin
- 2 enhance phytoplankton productivity in surface waters

- 4 De'Marcus Robinson^{1*}, Anh L.D. Pham¹, David J. Yousavich², Felix Janssen³, Frank
- 5 Wenzhöfer³, Eleanor C. Arrington⁴, Kelsey M. Gosselin⁵, Marco Sandoval-Belmar¹,
- 6 Matthew Mar¹, David L. Valentine⁴, Daniele Bianchi¹, Tina Treude^{1,2*}

7

- 8 ¹Department of Atmospheric and Oceanic Sciences, University of California Los Angeles, Los
- 9 Angeles, CA, USA
- ²Department of Earth, Planetary, and Space Sciences, University of California Los Angeles, Los
- 11 Angeles, CA, USA
- 12 ³HGF-MPG Joint Research Group for Deep-Sea Ecology and Technology, Alfred Wegener
- 13 Institute, Helmholtz Centre for Polar and Marine Research, Bremerhaven, Germany
- 14 ⁴Department of Earth Science and Marine Science Institute, University of California, Santa
- 15 Barbara, CA 93106, USA
- 16 ⁵Interepartment Graduate Program in Marine Science, University of California, Santa Barbara, CA
- 17 93106, USA

18

- 19 *Correspondence: De'Marcus Robinson, demarcus1.robinson@atmos.ucla.edu; Tina Treude,
- 20 ttreude@g.ucla.edu

21

Abstract

232425

26

27

28

29

30

31

32

33

34

35

36

37

38

39

40

41

42

The trace metal iron (Fe) is an essential micronutrient that controls phytoplankton productivity, which subsequently affects organic matter cycling with feedback on the cycling of macronutrients. Along the continental margin of the U.S. West Coast, high benthic Fe release has been documented, in particular from deep anoxic basins in the Southern California Borderland. However, the influence of this Fe release on surface primary production remains poorly understood. In the present study from the Santa Barbara Basin, in-situ benthic Fe fluxes were determined along a transect from shallow to deep sites in the basin. Fluxes ranged between 0.23 and 4.9 mmol m⁻² d⁻¹, representing some of the highest benthic Fe fluxes reported to date. To investigate the influence of benthic Fe release from the oxygen-deficient deep basin on surface phytoplankton production, we combined benthic flux measurements with numerical simulations using the Regional Ocean Model System coupled to the Biogeochemical Elemental Cycling model (ROMS-BEC). For this purpose, we updated the model Fe flux parameterization to include the new benthic flux measurements from the Santa Barbara Basin. Our simulations suggest that benthic Fe fluxes enhance surface primary production, supporting a positive feedback on benthic Fe release by decreasing oxygen in bottom waters. However, a reduction of phytoplankton Fe limitation by enhanced benthic fluxes near the coast may be partially compensated by increased nitrogen limitation further offshore, limiting the efficacy of this positive feedback.

1. Introduction

43

55

- 44 The California Current System (CCS), located off the coasts of Washington, Oregon, and 45 California, is a typical Eastern Boundary Upwelling System, where seasonal upwelling supports a highly diverse and productive marine ecosystem (Chavez and Messié, 2009; Carr and Kearns, 46 47 2003). The CCS can be split into three main parts: the main equatorward California Current 48 offshore, a subsurface poleward undercurrent fringing the continental shelf, and a recirculation 49 pattern known as the Southern California Eddy in the Southern California Bight. 50 In the CCS, both upwelling and large-scale circulation provide essential nutrients to the euphotic 51 zone, where they fuel high rates of net primary production (NPP). While seasonal upwelling 52 dominates north of Point Conception, advection by the CCS provides a major route for nutrient 53 supply to the Santa Barbara Channel in the Southern California Bight (Bray et al., 1999). Following 54 phytoplankton blooms, sinking and degradation of organic matter lead to oxygen consumption and
- Along the southern California coast, this oxygen depletion is exacerbated by regional circulation

widespread oxygen loss in subsurface waters (Brander et al., 2017; Chavez and Messié, 2009).

- 57 patterns that include transport of low-oxygen waters of tropical origin along the poleward
- undercurrent (Evans et al., 2020; Pozo Buil and Di Lorenzo, 2017). Oxygen decline is particularly
- 59 apparent in deep, isolated basins such as those found in the Southern California continental
- 60 borderland, where the presence of shallow sills limits ventilation of deep waters, and anoxic
- 61 conditions are often encountered near the bottom (Reimers et al., 1990; Goericke et al., 2015;
- 62 White et al., 2019).
- In the CCS, the trace metal iron (Fe) has been identified as a limiting factor for the growth of
- 64 phytoplankton (Hogle et al., 2018). Fe is an essential micronutrient that has also a considerable
- influence on the dynamics of phosphorus and nitrogen in the euphotic zone (Tagliabue et al., 2017).
- 66 Similar to other nutrients, Fe is transported to the surface by upwelling and circulation. However,
- Fe supply is generally low in oxygenated environments relative to other macronutrients, reflecting
- rapid scavenging of insoluble iron-oxide minerals by sinking particles that eventually accumulate
- in the sediment (Bruland et al., 2001, 2014; Firme et al., 2003; Till et al., 2019). While early studies
- suggested that Fe inputs to the CCS are dominated by rivers and aeolian deposition (Biller and
- Pruland, 2013; Johnson et al., 2003), more recent work highlights a combination of sources,

- 72 including benthic fluxes (Severmann et al., 2010; Noffke et al., 2012; Tagliabue et al., 2017;
- Wallmann et al., 2022) and ocean currents, which help redistributing Fe in coastal waters (Bray et
- 74 al., 1999; Boiteau et al., 2019; García-Reyes and Largier, 2010).
- 75 Benthic release of Fe(II), the reduced and soluble form of Fe, has been recognized as a potential
- source of Fe to the surface ocean along the continental shelf and slope of the CCS, including the
- deep basins of the California borderland (John et al., 2012; Severmann et al., 2010). Under hypoxic
- 78 or anoxic bottom waters, Fe(II) produced in the sediment during microbial organic matter
- 79 degradation coupled to Fe (III) reduction diffuses across the sediment-water interface and
- accumulates in the water column (Furrer and Wehrli, 1993; Dale et al., 2015; Severmann et al.,
- 81 2010; Wallmann et al., 2022). In the CCS, this benthic Fe flux is likely to exceed atmospheric
- deposition (Deutsch et al., 2021), and may ultimately make its way to the surface by upwelling
- and vertical mixing, supporting high rates of photosynthesis.

84 The interaction between low bottom water oxygen, Fe(II) release, and transport by the ocean 85 circulation is particularly important in the Santa Barbara Basin (SBB), an oxygen-deficient basin 86 located between the Channel Islands and mainland California in the Southern California Bight. 87 The SBB frequently experiences seasonal anoxia in the bottom water in fall, with irregular oxygen 88 flushing of dense, hypoxic water below the western sill depth (470 m) during winter and spring 89 (Goericke et al., 2015; Sholkovitz and Soutar, 1975; White et al., 2019; Qin et al., 2022). This 90 seasonal flushing reflects either changes in upwelling strength and frequency, or changes in 91 stratification at the sill depth, although the exact cause of the flushing is still unclear (Goericke et 92 al., 2015; Sholkovitz and Gieskes, 1971; White et al., 2019). Lack of oxygen in the deeper parts 93 of the basin supports anaerobic microbial processes in the bottom water and sediment (White et 94 al., 2019), including benthic Fe reduction (Goericke et al., 2015), causing the release of Fe(II) into 95 the water column (Severmann et al., 2010). Ventilation events that re-oxygenate the deep basin, as 96 well as mixing by the vigorous submesoscale circulation (Kessouri et al., 2020), could allow 97 upwelling of this Fe above the sill depth and ultimately to the surface, providing a linkage between 98 benthic processes and upper water-column biogeochemistry. Increased surface primary production 99 supported by this Fe source would in turn drive higher remineralization and oxygen loss in deep 100 waters, thus providing a positive feedback to benthic Fe release. However, with a dearth of benthic

Fe flux measurements in the SBB, gaps remain in our understanding of the dynamics and impact

of benthic Fe flux in the Southern California Borderland, particularly with respect to its magnitude, dependence on bottom water oxygen, and ability to reach the euphotic zone and influence primary production.

In this study, we explore the connection between benthic Fe flux and surface primary production in the CCS, by investigating the influence of enhanced benthic Fe fluxes from low-oxygen waters with a combination of field observations and experiments with a numerical model. We focus on the SBB, where we provide a new set of benthic Fe flux estimates determined by in-situ benthic flux chamber measurements. We combine these new observations with existing data (Severmann et al., 2010) to revise the representation of benthic Fe fluxes in UCLA's Regional Ocean Modeling System coupled to the Biogeochemical Elemental Cycling (ROMS-BEC) model (Deutsch et al., 2021). We then use the model to evaluate the effect of benthic Fe fluxes on surface nutrient consumption and NPP, and compare their impact to that of aeolian Fe deposition in the SBB and beyond.

2. Materials and Methods

2.1 Study Site

Fieldwork in the SBB was conducted between Oct 29 and Nov 11, 2019, during the R/V Atlantis cruise AT42-19. Sampling occurred during the anoxic, non-upwelling season along one bimodal transect with six stations total at depths between 447 and 585 m (Fig. 1, Table 1).

120

126

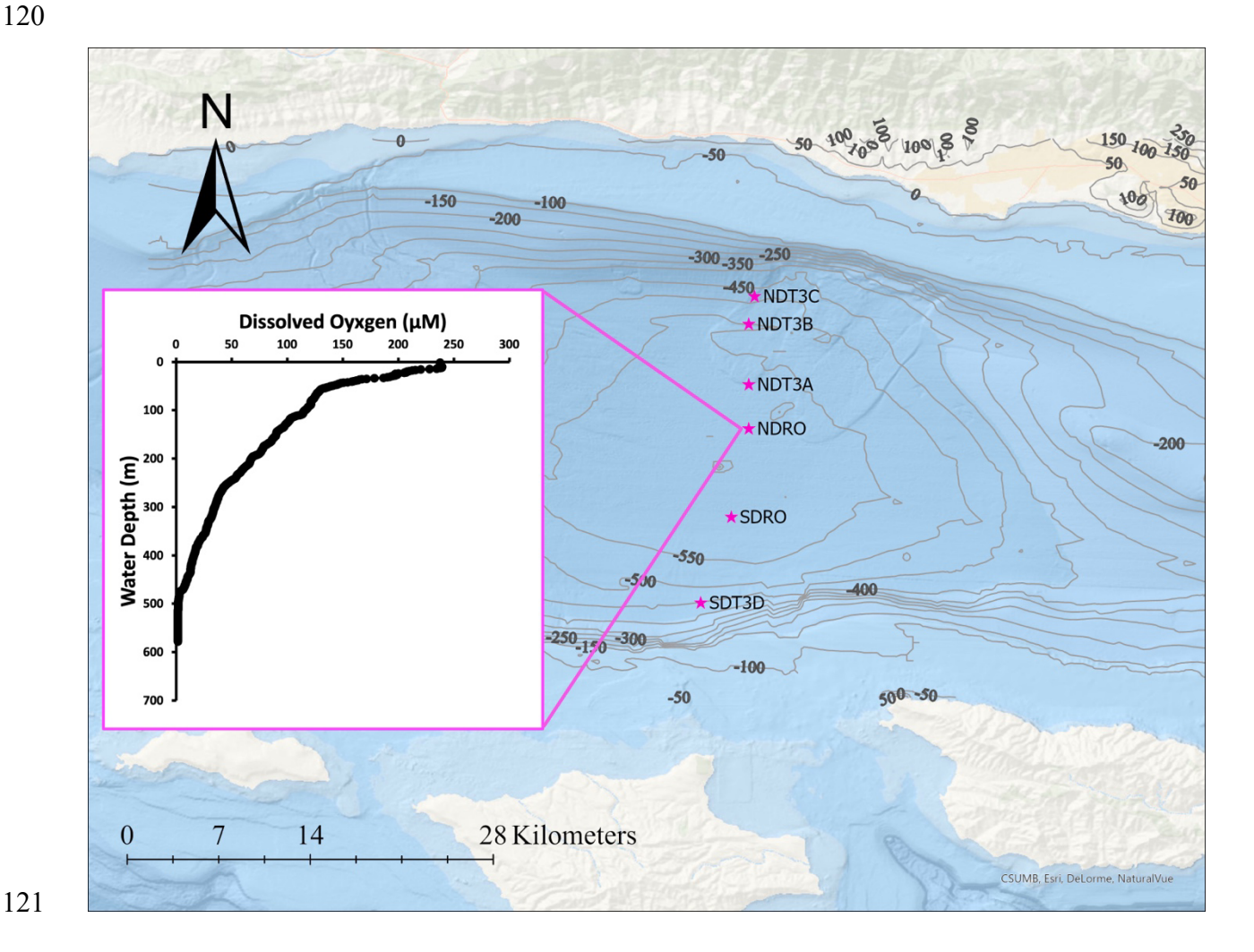
115

116

117

118

119



122 Figure 1. Station locations in the SBB during the AT42-19 expedition with R/V Atlantis. NDT3 123 (with stations A, B, C) = Northern Depocenter Transect Three, NDRO = Northern Depocenter 124 Radial Origin, SDRO = Southern Depocenter Radial Origin, SDT3 (with station D) = Southern 125 Depocenter Transect Three. The small insert figure displays dissolved oxygen concentrations in

the water column at the NDRO station profiled by an optical oxygen sensor attached to the AUV

- 127 Sentry. The profile was measured at the following position: Latitude 34.2618 N, Longitude -
- 128 120.0309 E. The map was created using ArcGIS Ocean Basemap, with bathymetric contour lines
- representing depth information taken from the General Bathymetric Chart of the Ocean (GEBCO)
- database.

155

- 131 Transects were divided into northern (NDT3 = Northern Depocenter Transect Three) and southern
- 132 (SDT3 = Southern Depocenter Transect Three) sites based on basin geography (Fig. 1). Stations
- were labeled alphabetically from A (deepest) to D (shallowest) according to their location along
- the transect, except for the deepest stations at the bottom of the basin, which were labeled Northern
- Depocenter Radial Origin (NDRO) and Southern Depocenter Radial Origin (SDRO).

2.2 Benthic Flux Chambers

137 Custom-built cylindrical benthic flux chamber systems (Treude et al., 2009) were deployed by the 138 ROV Jason at the six stations (Fig. 1). Polycarbonate chambers (19 cm inner diameter) were 139 installed in a small lightweight frame made from fiber-reinforced plastics. A stirrer (Type K/MT 140 111, K.U.M. Umwelt- und Meerestechnik, Kiel, Germany) was used to keep the water overlying 141 the sediment enclosed by the chamber well mixed. One or two replicate chamber systems were 142 deployed at each site. Since sediment in the SBB is quite soft and poorly consolidated, especially 143 towards the deeper stations, frames were fitted with platforms attached to the feet of the frame and 144 with buoyant syntactic foam to reduce sinking into the sediment. A syringe sampler was equipped 145 with 6 glass sampling syringes that were connected with 50 cm long plastic tubes (2.5mm inner 146 diameter, Vygon, Aachen, Germany). Each sampling syringe withdrew 50 mL of the overlying 147 seawater at pre-programmed times. A seventh syringe was used to inject 50 mL of de-ionized 148 water shortly after chambers were deployed to calculate chamber volume from the salinity-drop 149 recorded with a conductivity sensor (type 5860, Aanderaa Data Instruments, Bergen, NO) in the 150 overlying water, following the approach described in (Kononets et al., 2021). Water samples were 151 analyzed for Fe(II) on the ship using a Shimadzu UV-Spectrophotometer (UV-1800), equipped 152 with a sipper unit, following the procedure of (Grasshoff and Ehrhardt, 1999). Fe fluxes were 153 calculated from the slope of linear fits of Fe concentration time series vs. time (Fig. S1), multiplied 154 by the chamber volume, and divided by the surface area of the sediment (Kononets et al., 2021).

2.3 Numerical model (ROMS-BEC)

156 To explore the impacts of benthic Fe fluxes on surface primary production, we used a well-157 established ocean biogeochemical model of the CCS (Renault et al., 2016; Deutsch et al., 2021). 158 The physical model component consists of the Regional Ocean Modeling System (ROMS), 159 (Shchepetkin, 2015; Shchepetkin and McWilliams, 2005) a primitive-equation, hydrostatic, 160 topography-following ocean model. As in prior work, the model domain spans the entire U.S. West 161 Coast, from Baja California to Vancouver Island, with a horizontal resolution of 4 km, enough to 162 resolve the mesoscale circulation (Capet et al., 2008). The baseline model configuration was run 163 over the period 1995–2017 with interannually varying atmospheric forcings. We refer the reader 164 to earlier publications (Renault et al., 2021; Deutsch et al., 2021) for a complete description of the 165 model configuration, setup, forcings and boundary conditions used in this study.

166

167

168

169

170

171

172

173

174

175

176

177

178

179

180

181

182

183

184

185

186

ROMS is coupled online to the Biogeochemical Elemental Cycling (BEC) model (Moore et al., 2004), adapted for the U.S. West Coast by (Deutsch et al., 2021). BEC solves the equations for the evolution of six nutrients (nitrate (NO₃-), ammonium (NH₄+), nitrite (NO₂-), silicate (SiO₂), phosphate (PO₄³-), and iron (Fe)), three phytoplankton groups (small phytoplankton, diatoms, and diazotrophs), a single zooplankton group, inorganic carbon, oxygen (O2), and dissolved organic matter (carbon, nitrogen, phosphorus, and iron). Nutrient and carbon cycles are coupled by a fixed stoichiometry, except for silica and Fe, which use variable stoichiometries (Deutsch et al., 2021; Moore et al., 2001, 2004). The Fe cycle in BEC includes four separate pools: dissolved inorganic Fe (dFe), dissolved and particulate organic Fe, and Fe associated with mineral dust. Of these, only dissolved organic and inorganic Fe are explicitly tracked as state variables, while particulate Fe is treated implicitly by resolving vertical sinking particle fluxes (Moore et al., 2001; Moore and Braucher, 2008). Four main processes control the cycle of Fe in the model: atmospheric deposition, biological uptake and remineralization, scavenging by sinking particles, and release by sediment. The atmospheric dFe deposition is based on the dust climatology of (Mahowald et al., 2006), and dissolution rates from (Moore and Braucher, 2008). Different from (Deutsch et al., 2021), we reevaluated the dependence of benthic dFe fluxes on bottom water O2 concentrations in the California margin based on a merged dataset that combines our measurements from the SCB, with those presented in (Severmann et al., 2010) (see Section 2.5). The model Fe scavenging scheme removes dFe from the water column at a rate proportional to sinking particle fluxes and dFe concentrations, assuming a uniform concentration of 0.6 nM of Fe-binding ligands (Moore et al., 2004; Moore and Braucher, 2008). Accordingly, scavenging rates increase strongly at dFe

- 187 concentrations greater than 0.6 nM, and vice versa rates decrease strongly below 0.5 nM (Fig. S2).
- Note that, while simplistic, this formulation is still widely adopted by global ocean
- biogeochemistry models (Tagliabue et al., 2014, 2016), although improvements have been
- proposed (Moore and Braucher, 2008; Aumont et al., 2015; Pham and Ito, 2019, 2018).
- 191 As shown in previous work, the model captures the main patterns of physical and biogeochemical
- variability in the CCS, providing a representation of nutrient cycles and NPP in good agreement
- with observations (Renault et al., 2021; Deutsch et al., 2021). We further evaluate the model
- against an extended set of dissolved Fe measurements for the CCS (see Sections **2.4** and **3.1**).

2.4 Fe dataset along the U.S. West Coast

195

211

- To assess the ability of the model to capture observed patterns in dFe along the U.S. West Coast,
- we gathered available dFe concentration measurements from published studies, including a global
- 198 compilation (Tagliabue et al., 2016), regional programs such as CalCOFI, CCE-LTER, IRNBRU
- and MBARI cruises (Bundy et al., 2016; Hogle et al., 2018; Johnson et al., 2003; King and
- Barbeau, 2011), and other individual studies (Biller and Bruland, 2013; Boiteau et al., 2019; Bundy
- 201 et al., 2014, 2015, 2016; Chappell et al., 2019; Chase, 2002; Chase et al., 2005; Firme et al., 2003;
- Hawco et al., 2021; John et al., 2012; Till et al., 2019). In the final compilation, we define dFe as
- 203 the sum of the dissolved Fe and dissolvable Fe, based on the definitions used in each publication.
- Different studies used different filter sizes to define the dFe pool, most commonly 0.20, 0.40, and
- 205 0.45 μm, and different sampling methods, such as bottles, pump systems and/or surface tows. In
- some studies, samples were briefly acidified before being analyzed. Despite the differences in
- sampling and measurement approaches, we found that these datasets generally agreed with each
- other, suggesting that the final compilation accurately represents the dFe distribution along the
- 209 U.S. West Coast. The final dataset includes observations from 1980 to 2021, with most samples
- collected between 1997 and 2015, and from the upper 100 m of the water column.

2.5 Experimental Design

- To evaluate the impact of Fe fluxes from low-O₂ sediment in the SBB on surface biogeochemistry,
- 213 we designed a suite of model sensitivity experiments with ROMS-BEC in which external sources

- of Fe are modified relative to a baseline simulation. Accordingly, we run the following model
- 215 experiments:
- 216 *High-flux*: This experiment is the baseline model simulation, using a Fe flux parameterization
- 217 calculated as an exponential fit to a data set of benthic Fe fluxes consisting of the new benthic
- 218 measurements from AT42-19 and previous observations from the U.S. West Coast (Severmann et
- al., 2010) (see Section 3.2), thus updating the parameterization by (Deutsch et al., 2021). Benthic
- 220 Fe release follows the equation:
- $\log_{10}(\text{Fe}) = 2.86 0.01 \cdot O_2$ (Equation 1)
- Where O₂ is the concentration of oxygen in mmol m⁻³ and (Fe) is the Fe flux in μmol m⁻² d⁻¹. This
- revised formulation is only applied in the SBB where we performed our measurements, while a
- different formulation, solely based on data by (Severmann et al., 2010) is used outside of the SBB:
- $\log_{10}(\text{Fe}) = 2.6178 0.0128 \, \text{O}_2 \tag{Equation 2}$
- For this parameterization, we corrected a model bias that resulted in modeled bottom O₂
- 227 concentrations greater than 30 mmol m⁻³ over most of the deep basins where observations indicated
- lower concentrations, down to oxygen-free conditions (Fig. S3). We therefore reduced modeled
- bottom water O₂ concentrations in the Southern California Borderland by 30 mmol m⁻³, based on
- 230 the average difference between model and observed O₂ in the region. This correction is crucial to
- producing realistic benthic Fe fluxes under the anoxic conditions observed in the SBB, rather than
- 232 fluxes at O₂ concentrations of 30 mmol m⁻³.
- 233 *Hypoxia-off:* The purpose of this experiment is to evaluate the importance of enhanced Fe fluxes
- 234 under low-O₂ conditions in the SBB. Benthic Fe fluxes are calculated as in *High-flux* experiment
- 235 (Equation 2), but they are capped at a constant value when O₂ decreased below a threshold of 65
- 236 mmol m⁻³, which we chose as representative of hypoxic conditions (Deutsch et al., 2011). This
- change is applied only to in the SBB, and effectively bounds the benthic Fe release at 1.48 umol
- m^{-2} d⁻¹ when O₂ drops below the threshold for hypoxia.

239 **Dust-off:** The purpose of this experiment is to evaluate the importance of aeolian Fe deposition in 240 the CCS, and to compare it with the benthic Fe fluxes. In this experiment, the atmospheric Fe 241 deposition is set to zero; all other settings are identical to the *High-flux* experiment. 242 The baseline (High-flux) model simulation is run from 1995 to 2017. The other two model 243 sensitivity experiments (*Hypoxia-off* and *Dust-off*) are branched off from the *High-flux* simulation 244 in year 2008 and run separately for 10 additional years (2008-2017). All model experiments use 245 the same set of forcings and initial conditions. Results from the final 3 years (2015-2017) of the 246 Hypoxia-off and Dust-off simulations are averaged and analyzed by comparing differences in

biogeochemical fields (Fe, NO₃-, and NPP) to the final 3 years of the *High-flux* run.

3. Results

3.1 In-situ benthic Fe fluxes and model parameterization

Benthic Fe fluxes from in-situ benthic chamber measurements during the AT42-19 expedition are shown in **Table 1**. High Fe flux was recorded at the anoxic depocenter stations (4.90 and 3.92 mmol m⁻² d⁻¹ at SDRO and 3.49 mmol m⁻² d⁻¹ at NDRO). Fe fluxes at the shallower hypoxic stations (NDT3C, NDT3B, and SDT3D) were an order of magnitude lower. The Fe flux at the hypoxic NDT3A station between NDRO and NDT3B was approximately half the flux observed at the depocenter.

Table 1. Station details and geochemical parameters determined during the AT42-19 expedition. Benthic Fe fluxes were determined using in-situ benthic chambers. Dissolved O₂ concentrations were measured in the water column at 10 m above the seafloor using a Seabird optode sensor attached to the ROV Jason. At stations with two benthic chamber deployments (NDT3A and SDRO), O₂, geographical coordinates, and depth were averaged as there were only minimal differences between the two chamber deployments.

Station	Fe Flux [mmol m ⁻² d ⁻¹]	O ₂ [mmol m ⁻³]	Latitude [N]	Longitude [E]	Depth [m]
NDT3C	0.23 (n=1)	5.3	34.3526	-120.0160	499
NDT3B	0.36 (n=1)	6.8	34.3336	-120.0188	535
NDT3A	1.73; 1.20 (n=2)	9.6	34.2921	-120.0258	572
NDRO	3.49 (n=1)	0.0	34.2618	-120.0309	581
SDRO	4.90; 3.92 (n=2)	0.0	34.2011	-120.0446	586
SDT3D	0.58 (n=1)	9.6	34.1422	-120.0515	446

Trends in the Fe fluxes suggest modulation by O_2 concentration, water depth, and/or bathymetry. We also note that observed oxygen concentration represents a snapshot of bottom water conditions, while Fe fluxes likely reflect the oxygenation history at any given site. We observed a decrease in the Fe flux with a decrease in water depth (**Fig. 2**). There was also a slight trend of higher Fe fluxes with lower O_2 concentrations (most pronounced when O_2 reaches zero); however, since O_2

concentrations were relatively low at all stations (<10 mmol m⁻³) it is difficult to distill a clear pattern based on the small dataset. Notably, the NDT3A station showed a high Fe flux despite exhibiting the same O₂ concentration as the shallower station SDT3D. Basin bathymetry may also contribute to observed differences in the flux. For instance, the deeper depocenter and A-station showed higher averaged fluxes than the B, C, and D stations. We further noticed differences between the north and south extension of the transect. The southern stations (SDRO and SDT3D) showed a higher Fe flux than the northern stations (NDRO and NDT3C).

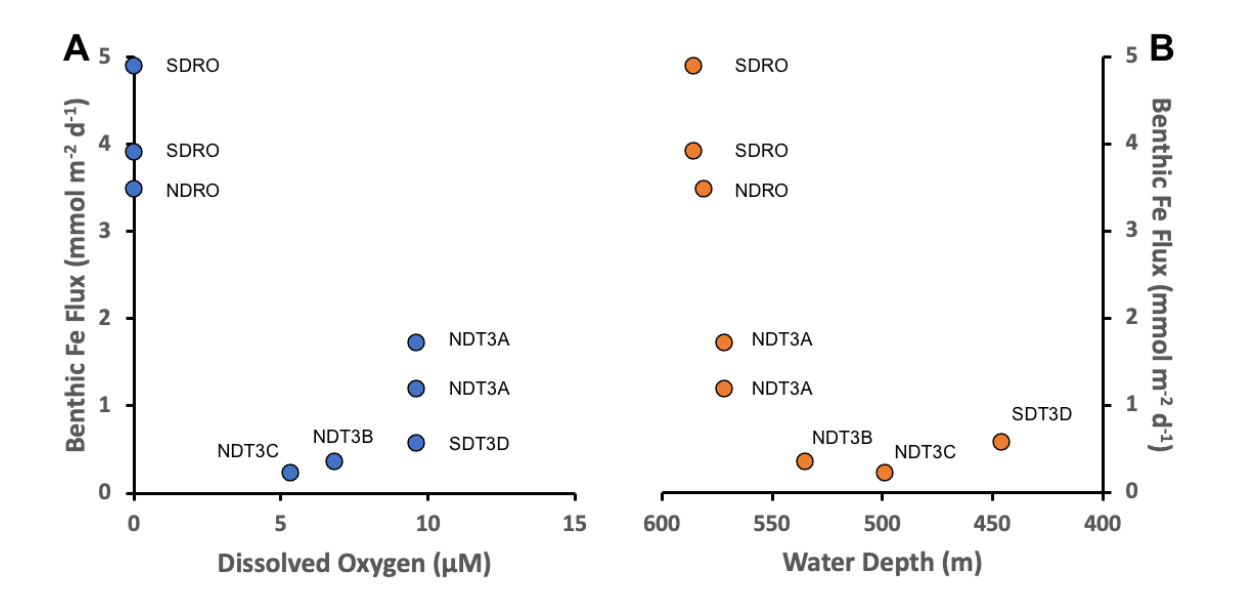


Figure 2. Benthic in-situ Fe fluxes. A: Fluxes as a function of O₂. B: Fluxes as a function of (station) water depth. Note that water depth is shown from deep to shallow depths. See Table 1 for station details.

We combined Fe fluxes determined during AT42-19 with previous estimates along the CCS, as compiled by (Severmann et al., 2010), and analyzed them as a function of bottom water O₂ (Fig. 3). Pooled together, the measurements can be described reasonably well by an exponential increase of Fe fluxes with declining bottom water O₂ (Severmann et al., 2010), although significant variability around an exponential fit remains. This relationship is consistent with the Fe flux parameterization adopted in the ROMS-BEC model (Deutsch et al., 2021). Several observations from the AT42-19 cruise (red dots in Fig. 3) exceed the range of previous measurements (blue dots in Fig. 3), likely owing to the anoxic or near-anoxic conditions in the water. Relative to the

exponential fit to the dataset by (Severmann et al., 2010) (yellow line in **Fig. 3**, see Equation 2) the revised fit to the pooled data (purple line in **Fig. 3**, see Equation 1) expands Fe fluxes by approximately a factor of two at O₂ concentrations close to zero, but decreases the magnitude of the Fe fluxes at concentrations above approximately 130 mmol m⁻³.

3.2 Model evaluation: High flux simulation

The *High-flux* simulation captures the magnitude and patterns of the observed dFe distribution in the upper ocean (**Fig. 4**), consistently with our knowledge of the ocean Fe cycle. In both model and observations, dFe concentrations are low at the surface, as a result of phytoplankton uptake, and increase gradually in subsurface waters due to organic matter remineralization in the water column and at the seafloor, and benthic Fe fluxes from the sediment (**Fig. S4**). The highest dFe concentrations are found along the coast, likely related to high surface productivity and shallow carbon export and remineralization, combined with basin bathymetry and O₂ deficiency. In the open ocean, dFe concentrations are low in both model and observations, reflecting a combination of phytoplankton uptake, scavenging by sinking particles, and low external inputs.

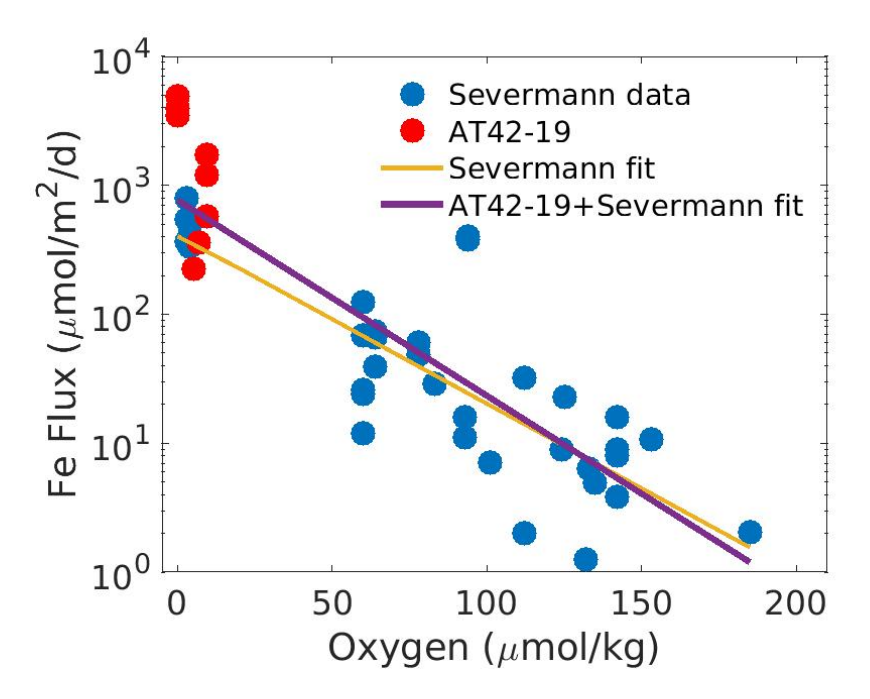


Figure 3. Combined benthic Fe flux data as a function of bottom oxygen. Blue dots show data from the compilation by (Severmann et al., 2010); red dots measurements from the AT42-19 cruise. The yellow line shows an exponential fits to the dataset by (Severmann et al., 2010)

(Equation 2). The purple line shows an exponential fit to the combined dataset (Equation 1). Note the logarithmic scale used for the y-axis.

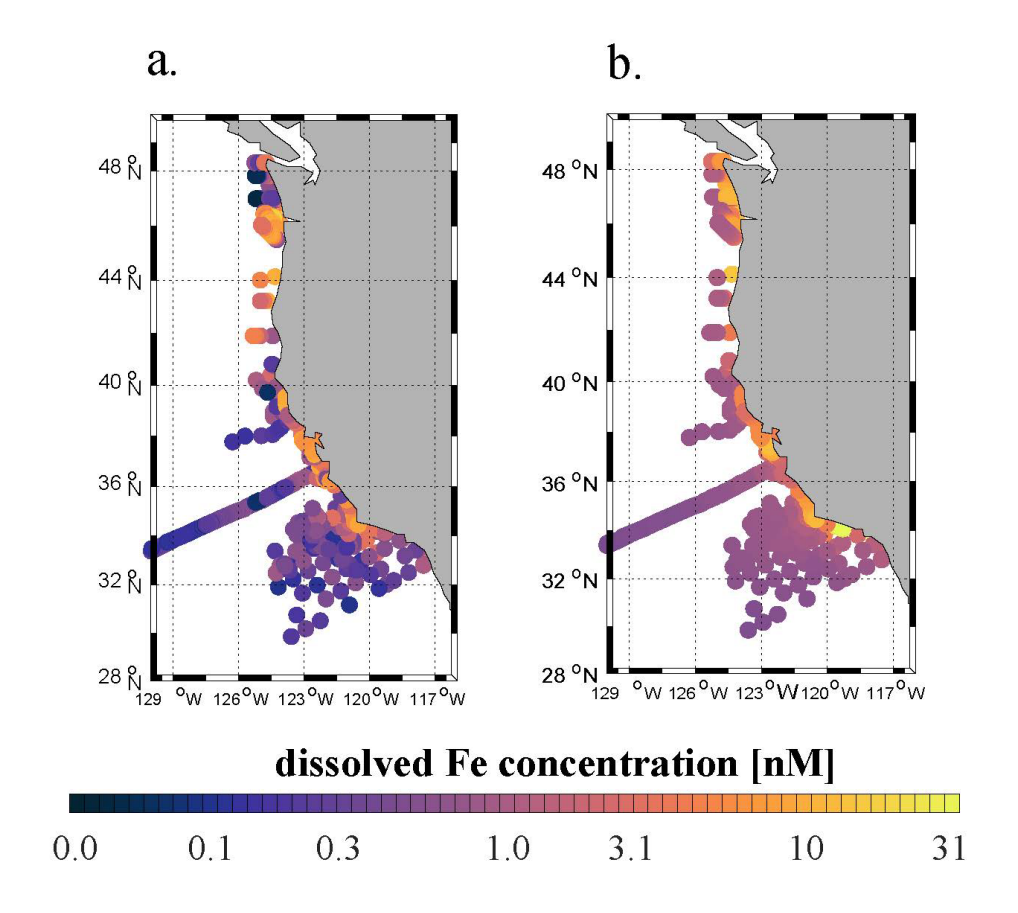


Figure 4. (a) Observed dFe concentrations (nM) from the U.S. West Coast compilation (see Section **2.4**) averaged between 0 and 100 m depth. (b) Annual mean modeled dFe concentrations (nM) averaged between 0 and 100 m depth, sampled at the same locations as the observations in panel (a).

Observational limitations prevent a more detailed validation of subsurface dFe patterns. Measurements of dFe concentrations in subsurface and deep waters (> 100 m) are currently very sparse in the CCS region and Southern California Borderland. Most of the dFe measurements for the SBB come from limited sampling conducted quarterly as part of selected CalCOFI (California Cooperative Oceanic Fisheries Investigations) cruises (King and Barbeau, 2011). These samples mostly focus on the mixed layer and are too sparse in space and time to capture the effects of deep-

319 water renewal events that ventilate the anoxic basins and allow uplifting and transport of deep 320 waters towards the surface. 321 The agreement of the model dFe with observations (correlation coefficient R=0.22, p<0.01) is 322 similar to that of other ocean biogeochemical models (Tagliabue et al., 2016). The model tends to 323 underestimate the sharp dFe gradient between coastal and open ocean waters, overestimating dFe 324 in the open ocean and producing too uniform concentrations offshore and at depth (Fig. 4). These 325 biases are likely related to the simple Fe scavenging scheme, which assumes a constant Fe-binding 326 ligand concentration of 0.6 nM. The small number and episodic nature of in-situ measurements 327 may also explain some of the mismatches between model and observations. 328 At the scale of the CCS, the *High-flux* simulation produces lower surface dFe in the southern part 329 of the domain (33°N to 36°N), and higher surface concentration in the northern part (40°N to 330 45°N) and near the central coast (Fig. 5a). While these patterns reflect a combination of internal 331 Fe cycling and external inputs, the elevated dFe in the northern CCS, in particular offshore, can be 332 partly attributed to higher aeolian deposition in that region (Fig. S5) as well as coastal inputs from 333 the Juan De Fuca strait (Deutsch et al., 2021). 334 The model reproduces the typical signature of coastal upwelling, with higher concentrations of 335 NO₃ nearshore in the central coast (36°N-40°N) and low concentrations in the Southern California 336 Bight and offshore (Fig. 5b). Similarly, the model reproduces high values of NPP near the coast, 337 in particular along the central coast, and rapidly decreasing values offshore (Fig. 5c). Relative to 338 previous modeling work (Deutsch et al., 2021) our simulations generate somewhat lower surface 339 NO₃ concentrations close to the coast, and sharper NPP gradients between the nearshore and 340 offshore regions, which are consistent with the rapid decrease in primary productivity and 341 chlorophyll shown by both satellite-based estimates and in situ data (Deutsch et al., 2021). These 342 changes likely reflect the higher benthic Fe fluxes in our simulations (Equation 1), which increase 343 phytoplankton productivity and promote nutrient drawdown near the coast.

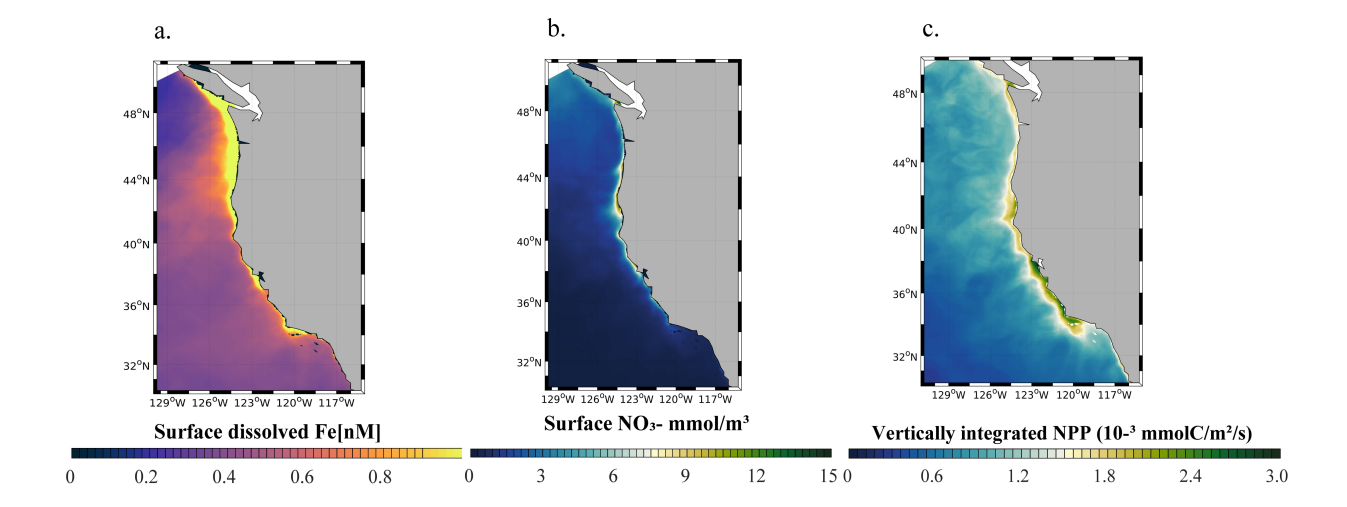


Fig. 5. (a) Surface dFe concentration, (b) surface NO₃⁻ concentration, and (c) vertically integrated net primary production (NPP) from the *High-flux* model simulation.

3.3 Hypoxia-off: Impact of benthic Fe flux from low-oxygen bottom water

We quantify the importance of benthic Fe fluxes from low-O₂ bottom waters in the Southern California Borderland by analyzing results from the *Hypoxia-off* experiment, in which we cap the high benthic Fe flux at a constant value (1.48 µmol m⁻² d⁻¹) when O₂ declines below hypoxic conditions (65 mmol m⁻³, see Section 2.5) (**Fig 6**).

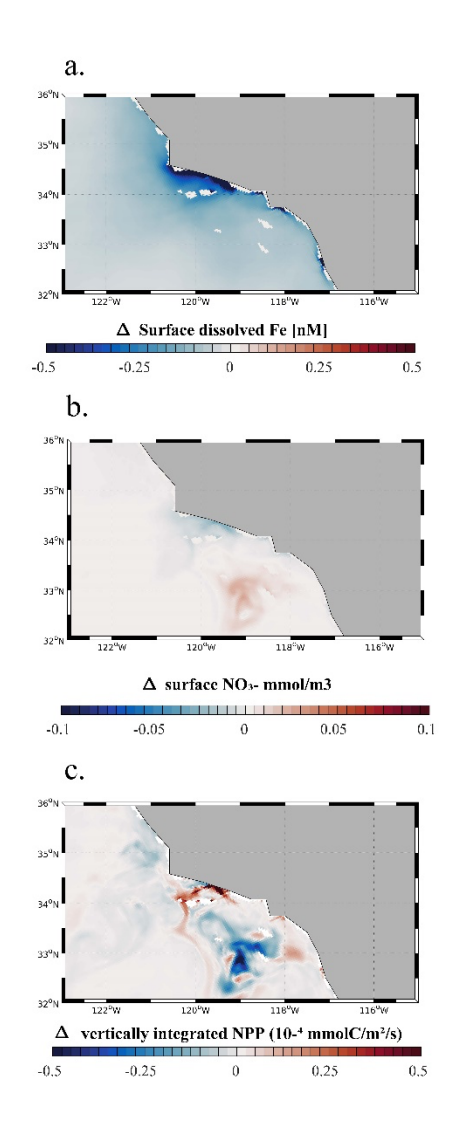


Figure 6. (a) Surface dFe anomalies, (b) Surface NO₃⁻ anomalies, and (c) vertically integrated net primary production (NPP) from the *Hypoxia-off* model run relative to the *High-flux* model run. The maps focus on the region around the SBB.

As expected, a decrease in benthic Fe flux from the anoxic basins in the *Hypoxia-off* simulation leads to a decrease in the surface dFe concentration (**Fig. 6a**). This decrease is particularly significant along the coast of the SBB, but also extends slightly into the open ocean (**Fig S6**). This trend indicates that dFe released from low-O₂ sediment is effectively transported to the surface and offshore, where it can affect primary production. The decrease in surface dFe caused by reduced benthic release causes a decline in NPP near the coast (**Fig. 6c**), where phytoplankton rely the most on benthic-derived Fe. NPP also shows a patchy increase in some regions,

especially between 32°N and 33°N and between 34°N and 35°N. This patchy increase can be explained by the relative importance of Fe vs. N limitation along a cross-shore productivity gradient. While near the SBB coast, phytoplankton is frequently Fe limited (up to 50% of the time in the model), especially following upwelling events, it tends to be almost exclusively N-limited moving offshore (Deutsch et al., 2021). This limitation pattern is consistent with observations from (King and Barbeau, 2011), who show that N:Fe ratios decrease moving from the coast to the open ocean (i.e., N is likely more limiting than Fe offshore). As Fe limitation reduces NPP near the coast in the *Hypoxia-off* experiment, NO₃- utilization also declines, so that more NO₃- can accumulate in surface waters (**Fig. 6b**). Shallow transport of excess NO₃- in mesoscale eddies can further fertilize offshore waters (Damien et al., 2023), releasing local N limitation and fueling an increase in NPP (**Fig. 6c**).

3.4 Dust-off: Role of atmospheric Fe deposition

We evaluate the importance of aeolian Fe sources in the *Dust-off* simulation, in which atmospheric Fe deposition is set to zero. In this experiment, surface dFe decreases everywhere in the CCS, but the decrease is particularly evident in the open ocean and the northern part of the domain (**Fig. 7a**). This dFe decrease leads to a widespread reduction in NPP in the northern CCS (40°N to 48°N, **Fig. 7c**), with stronger negative anomalies away from the coast. The decline in NPP is accompanied by a broad decrease in NO₃⁻ utilization, particularly evident offshore, where phytoplankton rely mostly on Fe delivery by dust. In contrast, we observe a broad increase in NPP in the southern CCS (south of 40°S) and in coastal areas, likely reflecting increased availability of NO₃⁻ transported southward by the broad California Current. The response of NPP in coastal areas and the southern CCS, when the dust deposition of Fe is set to zero, demonstrates that phytoplankton in those regions relies mostly on benthic Fe fluxes, rather than dust deposition, as the main source of Fe.

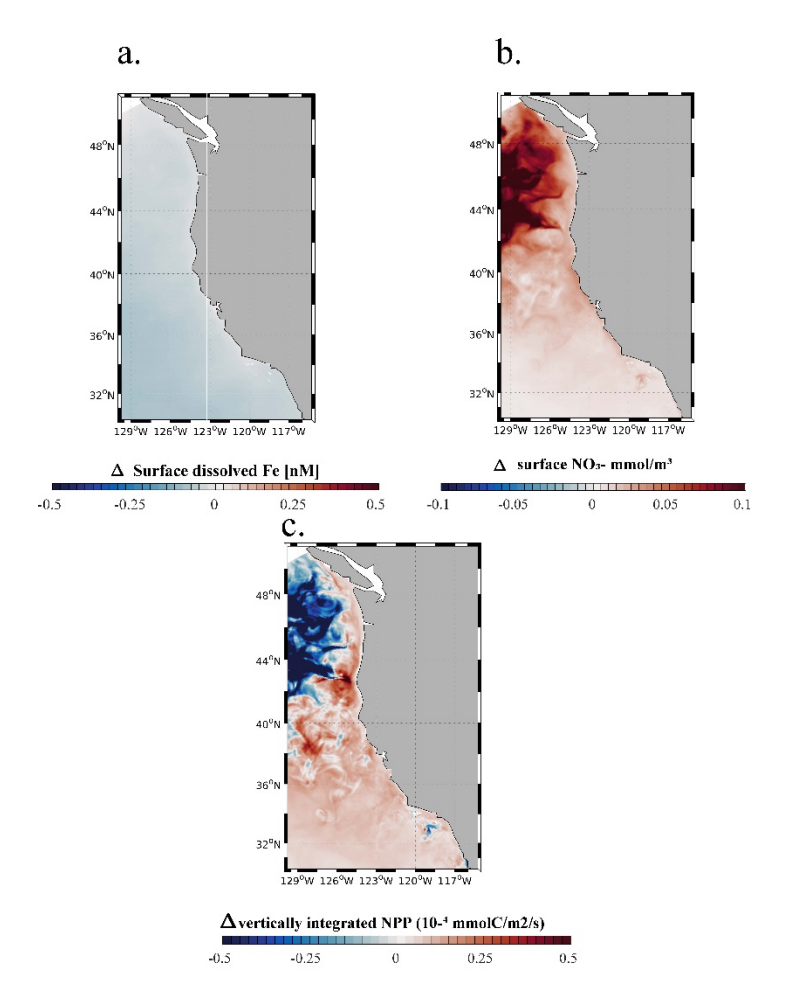
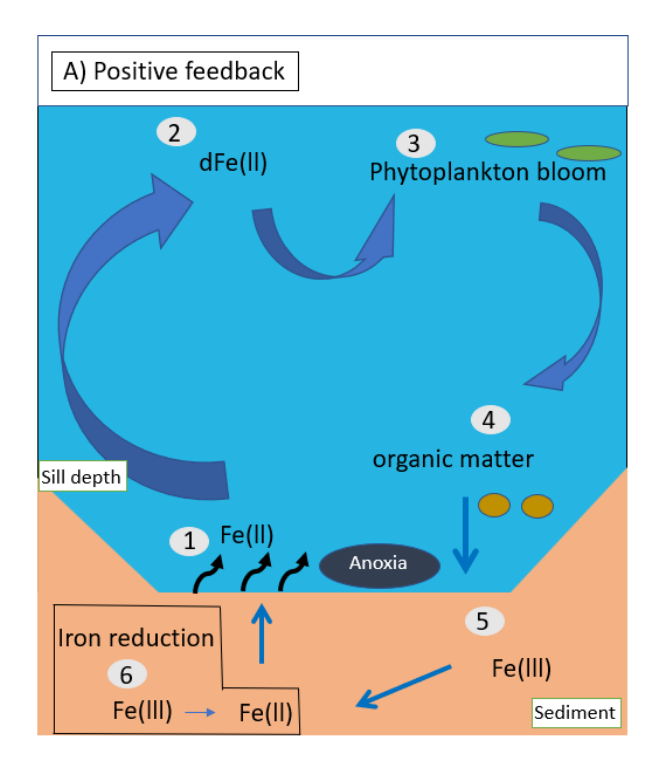


Figure 7. (a) Surface dissolved Fe, (b) surface NO_3^- anomalies, and (c) vertically integrated net primary production (NPP) from the *Dust-off* model run relative to the *High-flux* model run.

4. Discussion

4.1 Benthic Fe flux feedbacks on SBB biogeochemistry

The influence of bottom water O₂ concentration on the exchange of solutes between the sediment and the water column has been well documented (Soetaert et al., 2000; Sommer et al., 2016; Testa et al., 2013). Under hypoxic or anoxic bottom water conditions, organic matter sedimentation sustains anaerobic respiration at the sediment-water interface and in the sediment (Furrer and Wehrli, 1993; Middelburg and Levin, 2009a). Reduced compounds accumulate in pore waters forming chemical gradients (Widdows and Brinsley, 2002) that result in the flux of solutes such as Fe(II) out of the sediment, and their accumulation in bottom water (Jørgensen and Nelson, 2004; McMahon and Chapelle, 1991; Middelburg and Levin, 2009b; Yao et al., 2016). Similar conditions are observed in the SBB, where high sedimentation rates, water column denitrification below the sill depth, and high pore-water concentrations of sulfide and Fe(II) have been observed (Behl and Kennett, 1996; Bray et al., 1999; Goericke et al., 2015; Sholkovitz and Soutar, 1975; Sigman et al., 2003; White et al., 2019).



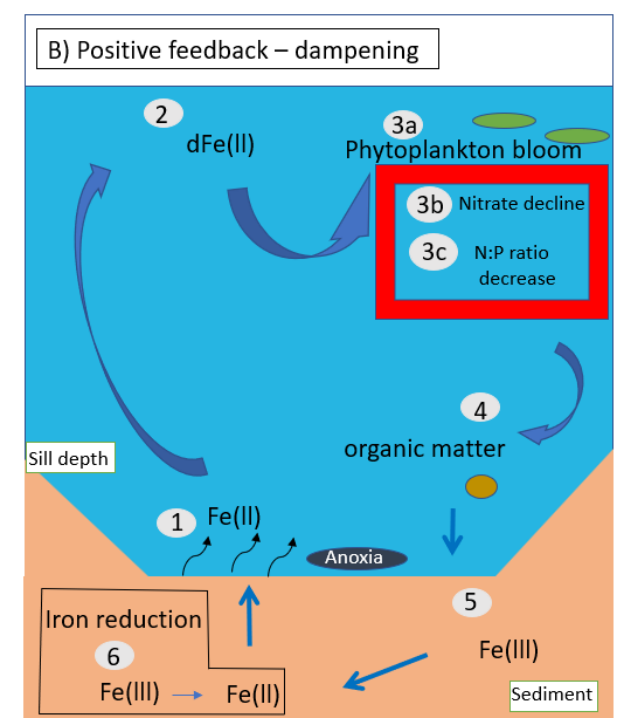


Figure 8. Schematic illustrating feedback loops between benthic Fe release, nutrient cycles, and productivity in the Santa Barbara Basin. (a) Positive feedback loop: 1. Benthic Fe is released into the oxygen-poor bottom water. 2. Upwelled Fe reaches the surface ocean increasing dissolved Fe concentrations. 3. Dissolved Fe is assimilated by phytoplankton, fueling blooms and production of organic matter and siderophores, i.e., ligands used to chelate ferric iron. 4. Organic matter is exported from the surface to the deep ocean. 5. Organic matter accumulates at the sediment-water interface. 6. During remineralization, iron-reducing bacteria reduce Fe(III) to Fe(II), increasing benthic dFe release. (b) Positive feedback loop – dampening: 1-3 (not including 3b and 3c) and 4-6 are identical to (a). Parts 3b and 3c illustrate the decline of NO₃⁻ at the surface caused by the reduction in Fe limitation, which together with increased denitrification in anoxic waters and sediment would limit the potential increase in primary production and export from the surface caused by Fe fertilization. Together with enhanced release of phosphate from anoxic sediment, a reduction in the available NO₃⁻ could also reduce the N:P ratio of phytoplankton. Ultimately, the effect of a decrease of NO₃⁻ on export and remineralization of organic matter would limit the increase of benthic Fe(II) fluxes, dampening the positive feedback.

The intense flux of dFe from the sediment suggests the potential for biogeochemical feedbacks in the SBB and more broadly in the CCS (as shown by Figs. 5-7). Under a positive feedback scenario (illustrated in Fig. 8a), anoxic and nearly anoxic bottom water conditions facilitate Fe(II) diffusion from the sediment into the bottom water. In the SBB, this Fe eventually reaches the surface via upwelling and mixing processes, which are likely enhanced in the presence of complex bathymetry and islands in the Southern California Bight (Kessouri et al., 2020). This additional dFe input fertilizes coastal waters and increases primary production. Newly formed organic matter eventually sinks towards the seafloor as a rain of organic particles, supporting low-oxygen concentrations in the bottom water, and fueling anaerobic respiration, including Fe reduction, in the sediment. This chain of processes thus represents a positive feedback loop that maintains high Fe(II) release from the sediment, as long as the bottom water remains hypoxic or anoxic (Mills et al., 2004; Noffke et al., 2012; Sañudo-Wilhelmy et al., 2001; Dale et al., 2015; Wallmann et al., 2022). Our simulations also indicate the potential for complex biogeochemical responses between Fe, NO₃ and NPP, which could limit the effects of these feedbacks. Specifically, the positive feedback loop is damped in our conceptual model by increased NO₃-limitation and elevated N-loss in anoxic sediments under oxygen-deficient bottom waters at higher Fe supply (illustrated by Fig. 8b), which would in turn limit the increase in NPP. Transport of N-depleted coastal waters can further reduce NPP offshore, counteracting the positive feedback. In addition, the positive feedback would be also damped by Fe scavenging, which is magnified at high dissolved Fe concentrations, unless Febinding ligands also increase. This damping effect is particularly strong in our model, where a constant ligand concentration of 0.6 nM is used, above which scavenging rapidly increases (Section 2). Such a negative feedback between scavenging and benthic Fe fluxes is consistent with the global modeling study by Somes et al. (2021).

429

430

431

432

433

434

435

436

437

438

439

440

441

442

443

444

445

446

447

448

449

450

451

452

453

454

455

456

457

458

Additional processes may further modulate these feedback loops. Increased anoxia in bottom water and sediment favors the removal of fixed N by denitrification (Goericke et al., 2015; White et al., 2019). Upwelling of NO₃-depleted waters would then reduce surface productivity by increasing N limitation (Gruber and Deutsch, 2014). Release of Fe(II) from the sediment could also impact phosphate dynamics. Phosphate is scavenged by Fe during oxidation of Fe(II) in the water column and sediment because of the ability of Fe(III) minerals to bind it. After burial, phosphate is released

due to reduction of solid Fe(III) minerals to dissolved Fe(II), and diffuses upward to be either readsorbed by Fe(III) at the oxic sediment-water interface, or released to the bottom water under anoxic conditions (Dijkstra et al., 2014). The latter scenario is consistent with our in-situ benthic flux chamber measurements revealing increased phosphate release from the sediment with increased depth in the SBB (Yousavich et al., 2023). Higher release of phosphate into the water column, and transport to the surface, could decrease the N:P ratio of phytoplankton, especially downstream of waters where denitrification occurred (Deutsch et al., 2007). In the presence of N limitation, these conditions could favor the activity of nitrogen-fixing microorganisms (Mills et al., 2004; Noffke et al., 2012; Sañudo-Wilhelmy et al., 2001), which could further modulate surface NPP (Deutsch et al., 2007).

4.2 Contribution of physical transport on surface Fe

Our numerical experiments suggest that Fe released into the deep SBB can reach surface waters and fertilize them. This finding highlights the critical role of bottom water upwelling and mixing in the deep basins of the Southern California Borderland. There is ample literature describing seasonal surface circulation and bottom water renewal and their effect on nutrients in the SBB (Bray et al., 1999; Hendershott and Winant, 1996; Sholkovitz and Gieskes, 1971). However, the frequency and rate of seasonal bottom water flushing events, and the processes responsible for vertical mixing and upwelling across hundreds of meters remain poorly understood (Shiller et al., 1985; Sholkovitz and Gieskes, 1971; White et al., 2019). It is likely that interaction between wind-driven upwelling events and submesoscale eddies, which are particularly intense inside the Santa Barbara Channel (Kessouri et al., 2020), favors upward mixing of deep bottom water in the wake of flushing events, connecting deep bottom waters to the surface.

4.3 Quantifying expansion of anoxia in the SBB

Changes in source waters and global O₂ loss have contributed to decreasing O₂ levels throughout the Southern California Bight and the SBB (Zhou et al., 2022). With the outlook of a continuing decline in oceanic O₂ (Bopp et al., 2013; Kwiatkowski et al., 2020), quantifying the expansion of hypoxic and anoxic zones in the SBB is vital to understand the dynamics and fate of Fe(II) and other reduced compounds, such as ammonium and hydrogen sulfide, in deep low-oxygen waters. In the SBB, bottom water renewal events have experienced a decline in frequency and magnitude,

driving an expansion of hypoxic and anoxic conditions in deep waters (White et al., 2019). This expansion has led to an increase in anaerobic reactions, such as denitrification in the water column (White et al., 2019) as well as sulfur cycling in the sediment (Valentine et al., 2016). Expansion of low O₂ waters could intensify the positive feedback loop between Fe release, NPP and O₂ loss (**Fig. 8**). However, to date, despite growing evidence for more frequent anoxia, there is no clear quantitative record of the vertical or horizontal expansions of oxygen-deficient waters in the SBB.

5. Conclusion

Our field campaign in the SBB measured a remarkably high flux of Fe(II) from the sediment (0.23 – 4.9 mmol m⁻² d⁻¹), greater than in previous studies from this region (Severmann et al., 2010) and from other oxygen minimum zones (Dale et al. 2015; Homoky et al. 2021). While these observations are based on snapshots of O₂ and Fe fluxes, they have implications for the temporal variability of Fe supply. High benthic Fe fluxes are observed during the anoxic fall season, while seasonal flushing in winter and spring likely decreases them by increasing bottom water O₂ and Fe oxidation and retention near the sediment.

Using a series of simulations with an ocean biogeochemical model, we show that this high Fe release from deep, low-oxygen sediment can reach the surface and impact nutrients and productivity in the SBB and the Southern California Bight, where Fe is often limiting (Hogle et al., 2018). We also highlight the impacts of coastal Fe inputs on waters further offshore. While phytoplankton in coastal areas directly benefits from Fe fertilization, increased NO₃- utilization in coastal waters can increase N-limitation of phytoplankton further downstream in open-ocean areas. Thus, benthic Fe fluxes can modulate Fe and NO₃- limitation in ways that partially counteract one another along the cross-shore productivity gradient of the CCS. Our simulations also suggest that Fe inputs from atmospheric deposition are mostly important in the open ocean north of 40°N, where phytoplankton rely on Fe delivery by dust. However, we also show that changes in atmospheric Fe deposition can affect ocean productivity in the southern CCS by altering NO₃- utilization further downstream. Our results support the idea that benthic Fe fluxes are the major source of Fe in the southern CCS and are supplemented by atmospheric deposition in northwestern and offshore waters, leading to relatively high NPP coastwide.

We suggest that benthic Fe fluxes from deep anoxic basins reach the surface in the SBB, contributing to feedbacks between Fe and NO₃⁻ limitation and NPP. Specifically, high Fe fluxes from low-oxygen sediment support higher NPP near the coast, in turn leading to increased respiration and O₂ loss at depth, maintaining high Fe release. This positive feedback is damped by increased NO₃⁻ limitation, which reduces NPP downstream of coastal regions. This benthic-pelagic coupling demonstrates the importance of sediment-derived Fe fluxes on the coastal ecosystem of the CCS, and the role of vertical transport processes in connecting deep environments to surface

waters along continental margins. Our results are thus consistent with previous work from the Peruvian coastal upwelling (Wallmann et al., 2022), suggesting that oceanic O₂ loss could drive an increase in benthic Fe fluxes, enhancing local productivity and leading to further O₂ loss. This positive feedback could be stabilized by loss of fixed nitrogen under expanded anaerobic conditions.

It is likely that feedbacks of the type highlighted by (Wallmann et al., 2022) and our work in the SBB are at play more broadly along low-oxygen upwelling systems and coastal OMZ. Further studies should focus on the coupling between benthic processes and Fe and nutrient cycling in these regions. For example, fixed nitrogen loss by denitrification and enhanced release of phosphorous under low-oxygen bottom water are likely to further modulate these interactions. Seasonal studies based on stable isotope, radiotracer, and geochemical techniques are required to track the fate and transport of nutrients in low-O₂ coastal regions, clarifying the dynamics and sensitivities of the underlying microbial metabolisms. Ocean biogeochemical models for regional and global studies should incorporate new observations of benthic fluxes and their sensitivity to bottom O₂ and other environmental variables. This would expand the ability of models to better capture the effects of long-term oceanic O₂ loss, and the feedbacks between benthic nutrient fluxes and surface productivity.

540 Acknowledgements

- We thank the captain and crew of R/V Atlantis, the crew of ROV Jason, the crew of AUV Sentry,
- and the science party of research cruise AT42-19 for their technical and logistical support. We
- 543 thank Q. Qin, M. O'Beirne, A. Mazariegos, X. Moreno, and A. Eastman for assisting with
- shipboard analyses. Funding for this work was provided by the US National Science Foundation,
- NSF OCE-1829981 (to TT), OCE-1756947 and OCE-1830033 (to DLV), and OCE-2023493 (to
- DB and ALP). Computational resources were provided by the Expanse system at the San Diego
- 547 Supercomputer Center through allocation TG-OCE170017 from the Extreme Science and
- 548 Engineering Discovery Environment (XSEDE), which was supported by National Science
- Foundation grant 1548562.

Code availability

- 551 The physical and biogeochemical codes used for our simulations can be accessed at:
- 552 https://github.com/UCLA-ROMS/Code.
- The model output can be accessed through Zenodo: (link will be provided before publication)

554

555

565

550

Data availability

- In-situ benthic Fe flux data are accessible through the Biological & Chemical Oceanography Data
- Management Office (BCO-DMO) under the following DOI: 10.26008/1912/bco-dmo.896706.1.

558 Author contributions.

- DR, TT, DB, and AP conceived this study. DM, DJY, FJ, FW, ECA, KMG, DLV and TT
- 560 conducted the sampling at sea. DJY transformed and interpreted ROV Jason data. FJ and FW
- constructed and managed benthic flux chambers. DYJ and DR analyzed Fe(II) and assisted with
- the flux calculation. MM provided the compiled Fe measurements along the U.S. West Coast. AP
- and MS performed the model simulations. DR, DB, AP and TT wrote the manuscript with input
- from all co-authors.

Competing interests

- Some authors are members of the editorial board of Biogeosciences. The peer-review process was
- guided by an independent editor, and the authors have no other competing interests to declare.

568 References

- Aumont, O., Ethé, C., Tagliabue, A., Bopp, L., and Gehlen, M.: PISCES-v2: An ocean
- 570 biogeochemical model for carbon and ecosystem studies, Geosci. Model Dev., 8, 2465–2513,
- 571 https://doi.org/10.5194/gmd-8-2465-2015, 2015.
- Behl, R. J. and Kennett, J. P.: Brief interstadial events in the Santa Barbara basin, NE Pacific,
- during the past 60 kyr, Nature, 379, 243–246, https://doi.org/10.1038/379243a0, 1996.
- Biller, D. V. and Bruland, K. W.: Sources and distributions of Mn, Fe, Co, Ni, Cu, Zn, and Cd
- 575 relative to macronutrients along the central California coast during the spring and summer
- 576 upwelling season, Mar. Chem., 155, 50–70, https://doi.org/10.1016/j.marchem.2013.06.003,
- 577 2013.
- Boiteau, R. M., Till, C. P., Coale, T. H., Fitzsimmons, J. N., Bruland, K. W., and Repeta, D. J.:
- Patterns of iron and siderophore distributions across the California Current System, Limnol.
- 580 Oceanogr., 64, 376–389, https://doi.org/10.1002/lno.11046, 2019.
- Bopp, L., Resplandy, L., Orr, J. C., Doney, S. C., Dunne, J. P., Gehlen, M., Halloran, P., Heinze,
- 582 C., Ilyina, T., Séférian, R., Tjiputra, J., and Vichi, M.: Multiple stressors of ocean ecosystems in
- the 21st century: projections with CMIP5 models, Biogeosciences, 10, 6225–6245,
- 584 https://doi.org/10.5194/bg-10-6225-2013, 2013.
- Brander, K., Cochrane, K., Barange, M., and Soto, D.: Climate Change Implications for Fisheries
- and Aquaculture, in: Climate Change Impacts on Fisheries and Aquaculture, edited by: Phillips,
- 587 B. F. and Pérez-Ramírez, M., John Wiley & Sons, Ltd, Chichester, UK, 45–62,
- 588 https://doi.org/10.1002/9781119154051.ch3, 2017.
- Bray, N. A., Keyes, A., and Morawitz, W. M. L.: The California Current system in the Southern
- 590 California Bight and the Santa Barbara Channel, J. Geophys. Res. Oceans, 104, 7695–7714,
- 591 https://doi.org/10.1029/1998JC900038, 1999.
- Bruland, K. W., Rue, E. L., and Smith, G. J.: Iron and macronutrients in California coastal
- 593 upwelling regimes: Implications for diatom blooms, Limnol. Oceanogr., 46, 1661–1674,
- 594 https://doi.org/10.4319/lo.2001.46.7.1661, 2001.
- Bruland, K. W., Middag, R., and Lohan, M. C.: Controls of Trace Metals in Seawater, in:
- 596 Treatise on Geochemistry, Elsevier, 19–51, https://doi.org/10.1016/B978-0-08-095975-7.00602-
- 597 1, 2014.
- Bundy, R. M., Biller, D. V., Buck, K. N., Bruland, K. W., and Barbeau, K. A.: Distinct pools of
- dissolved iron-binding ligands in the surface and benthic boundary layer of the California
- 600 Current, Limnol. Oceanogr., 59, 769–787, https://doi.org/10.4319/lo.2014.59.3.0769, 2014.
- Bundy, R. M., Abdulla, H. A. N., Hatcher, P. G., Biller, D. V., Buck, K. N., and Barbeau, K. A.:
- Iron-binding ligands and humic substances in the San Francisco Bay estuary and estuarine-

- influenced shelf regions of coastal California, Mar. Chem., 173, 183–194,
- 604 https://doi.org/10.1016/j.marchem.2014.11.005, 2015.
- Bundy, R. M., Jiang, M., Carter, M., and Barbeau, K. A.: Iron-Binding Ligands in the Southern
- 606 California Current System: Mechanistic Studies, Front. Mar. Sci., 3,
- 607 https://doi.org/10.3389/fmars.2016.00027, 2016.
- 608 Capet, X., Campos, E. J., and Paiva, A. M.: Submesoscale activity over the Argentinian shelf,
- 609 Geophys. Res. Lett., 35, https://doi.org/10.1029/2008GL034736, 2008.
- 610 Carr, M.-E. and Kearns, E. J.: Production regimes in four Eastern Boundary Current systems,
- 611 Deep Sea Res. Part II Top. Stud. Oceanogr., 50, 3199–3221,
- 612 https://doi.org/10.1016/j.dsr2.2003.07.015, 2003.
- 613 Chappell, P., Armbrust, E., Barbeau, K., Bundy, R., Moffett, J., Vedamati, J., and Jenkins, B.:
- Patterns of diatom diversity correlate with dissolved trace metal concentrations and longitudinal
- position in the northeast Pacific coastal-offshore transition zone, Mar. Ecol. Prog. Ser., 609, 69–
- 86, https://doi.org/10.3354/meps12810, 2019.
- 617 Chase, Z.: Iron, nutrient, and phytoplankton distributions in Oregon coastal waters, J. Geophys.
- 618 Res., 107, 3174, https://doi.org/10.1029/2001JC000987, 2002.
- 619 Chase, Z., Johnson, K. S., Elrod, V. A., Plant, J. N., Fitzwater, S. E., Pickell, L., and Sakamoto,
- 620 C. M.: Manganese and iron distributions off central California influenced by upwelling and shelf
- 621 width, Mar. Chem., 95, 235–254, https://doi.org/10.1016/j.marchem.2004.09.006, 2005.
- 622 Chavez, F. P. and Messié, M.: A comparison of Eastern Boundary Upwelling Ecosystems, Prog.
- 623 Oceanogr., 83, 80–96, https://doi.org/10.1016/j.pocean.2009.07.032, 2009.
- Dale, A. W., Nickelsen, L., Scholz, F., Hensen, C., Oschlies, A., and Wallmann, K.: A revised
- 625 global estimate of dissolved iron fluxes from marine sediments: GLOBAL BENTHIC IRON
- 626 FLUXES, Glob. Biogeochem. Cycles, 29, 691–707, https://doi.org/10.1002/2014GB005017,
- 627 2015.
- Damien, P., Bianchi, D., McWilliams, J. C., Kessouri, F., Deutsch, C., Chen, R., and Renault, L.:
- 629 Enhanced Biogeochemical Cycling Along the U.S. West Coast Shelf, Glob. Biogeochem.
- 630 Cycles, 37, e2022GB007572, https://doi.org/10.1029/2022GB007572, 2023.
- Deutsch, C., Sarmiento, J. L., Sigman, D. M., Gruber, N., and Dunne, J. P.: Spatial coupling of
- nitrogen inputs and losses in the ocean, Nature, 445, 163–167,
- 633 https://doi.org/10.1038/nature05392, 2007.
- 634 Deutsch, C., Brix, H., Ito, T., Frenzel, H., and Thompson, L.: Climate-Forced Variability of
- Ocean Hypoxia, Science, 333, 336–339, https://doi.org/10.1126/science.1202422, 2011.
- Deutsch, C., Frenzel, H., McWilliams, J. C., Renault, L., Kessouri, F., Howard, E., Liang, J.-H.,
- Bianchi, D., and Yang, S.: Biogeochemical variability in the California Current System, Prog.
- 638 Oceanogr., 196, 102565, https://doi.org/10.1016/j.pocean.2021.102565, 2021.

- 639 Dijkstra, N., Kraal, P., Kuypers, M. M. M., Schnetger, B., and Slomp, C. P.: Are Iron-Phosphate
- Minerals a Sink for Phosphorus in Anoxic Black Sea Sediments?, PLOS ONE, 9, e101139,
- 641 https://doi.org/10.1371/journal.pone.0101139, 2014.
- Evans, N., Schroeder, I. D., Pozo Buil, M., Jacox, M. G., and Bograd, S. J.: Drivers of
- Subsurface Deoxygenation in the Southern California Current System, Geophys. Res. Lett., 47,
- 644 https://doi.org/10.1029/2020GL089274, 2020.
- Firme, G. F., Rue, E. L., Weeks, D. A., Bruland, K. W., and Hutchins, D. A.: Spatial and
- 646 temporal variability in phytoplankton iron limitation along the California coast and consequences
- 647 for Si, N, and C biogeochemistry: SPATIAL AND TEMPORAL VARIABILITY IN
- 648 PHYTOPLANKTON IRON, Glob. Biogeochem. Cycles, 17,
- 649 https://doi.org/10.1029/2001GB001824, 2003.
- Furrer, G. and Wehrli, B.: Biogeochemical processes at the sediment-water interface:
- measurements and modeling, Appl. Geochem., 8, 117–119, https://doi.org/10.1016/S0883-
- 652 2927(09)80021-8, 1993.
- 653 García-Reyes, M. and Largier, J.: Observations of increased wind-driven coastal upwelling off
- 654 central California, J. Geophys. Res., 115, C04011, https://doi.org/10.1029/2009JC005576, 2010.
- 655 Goericke, R., Bograd, S. J., and Grundle, D. S.: Denitrification and flushing of the Santa Barbara
- Basin bottom waters, Deep Sea Res. Part II Top. Stud. Oceanogr., 112, 53–60,
- 657 https://doi.org/10.1016/j.dsr2.2014.07.012, 2015.
- 658 Grasshoff, K. and Ehrhardt, M.: Methods of seawater analysis, 3rd, completely rev. and extended
- ed. ed., Wiley-VCH, Weinheim, New York, xxxii, 600 pp., 1999.
- Hawco, N. J., Barone, B., Church, M. J., Babcock-Adams, L., Repeta, D. J., Wear, E. K.,
- Foreman, R. K., Björkman, K. M., Bent, S., Van Mooy, B. A. S., Sheyn, U., DeLong, E. F.,
- Acker, M., Kelly, R. L., Nelson, A., Ranieri, J., Clemente, T. M., Karl, D. M., and John, S. G.:
- Iron Depletion in the Deep Chlorophyll Maximum: Mesoscale Eddies as Natural Iron
- 664 Fertilization Experiments, Glob. Biogeochem. Cycles, 35,
- https://doi.org/10.1029/2021GB007112, 2021.
- Hendershott and Winant: Surface Circulation in the Santa Barbara Channel, Oceanography, 9,
- 667 114–121, https://doi.org/10.5670/oceanog.1996.14, 1996.
- Hogle, S. L., Dupont, C. L., Hopkinson, B. M., King, A. L., Buck, K. N., Roe, K. L., Stuart, R.
- K., Allen, A. E., Mann, E. L., Johnson, Z. I., and Barbeau, K. A.: Pervasive iron limitation at
- 670 subsurface chlorophyll maxima of the California Current, Proc. Natl. Acad. Sci., 115, 13300–
- 671 13305, https://doi.org/10.1073/pnas.1813192115, 2018.
- Homoky, W. B., Conway, T. M., John, S. G., König, D., Deng, F., Tagliabue, A., and Mills, R.
- A.: Iron colloids dominate sedimentary supply to the ocean interior, Proc. Natl. Acad. Sci., 118,
- 674 e2016078118, https://doi.org/10.1073/pnas.2016078118, 2021.

- John, S. G., Mendez, J., Moffett, J., and Adkins, J.: The flux of iron and iron isotopes from San
- 676 Pedro Basin sediments, Geochim. Cosmochim. Acta, 93, 14–29,
- 677 https://doi.org/10.1016/j.gca.2012.06.003, 2012.
- Johnson, K. S., Elrod, V. A., Fitzwater, S. E., Plant, J. N., Chavez, F. P., Tanner, S. J., Gordon,
- R. M., Westphal, D. L., Perry, K. D., Wu, J., and Karl, D. M.: Surface ocean-lower atmosphere
- interactions in the Northeast Pacific Ocean Gyre: Aerosols, iron, and the ecosystem response,
- 681 Glob. Biogeochem. Cycles, 17, https://doi.org/10.1029/2002GB002004, 2003.
- Jørgensen, B. B. and Nelson, D. C.: Sulfide oxidation in marine sediments: Geochemistry meets
- 683 microbiology, in: Sulfur Biogeochemistry Past and Present, Geological Society of America,
- 684 https://doi.org/10.1130/0-8137-2379-5.63, 2004.
- Kessouri, F., Bianchi, D., Renault, L., McWilliams, J. C., Frenzel, H., and Deutsch, C. A.:
- 686 Submesoscale Currents Modulate the Seasonal Cycle of Nutrients and Productivity in the
- 687 California Current System, Glob. Biogeochem. Cycles, 34, e2020GB006578,
- 688 https://doi.org/10.1029/2020GB006578, 2020.
- King, A. L. and Barbeau, K. A.: Dissolved iron and macronutrient distributions in the southern
- 690 California Current System, J. Geophys. Res., 116, C03018,
- 691 https://doi.org/10.1029/2010JC006324, 2011.
- Kononets, M., Tengberg, A., Nilsson, M., Ekeroth, N., Hylén, A., Robertson, E. K., van de
- Velde, S., Bonaglia, S., Rütting, T., Blomqvist, S., and Hall, P. O. J.: In situ incubations with the
- 694 Gothenburg benthic chamber landers: Applications and quality control, J. Mar. Syst., 214,
- 695 103475, https://doi.org/10.1016/j.jmarsys.2020.103475, 2021.
- 696 Kwiatkowski, L., Torres, O., Bopp, L., Aumont, O., Chamberlain, M., Christian, J. R., Dunne, J.
- 697 P., Gehlen, M., Ilyina, T., John, J. G., Lenton, A., Li, H., Lovenduski, N. S., Orr, J. C., Palmieri,
- 698 J., Santana-Falcón, Y., Schwinger, J., Séférian, R., Stock, C. A., Tagliabue, A., Takano, Y.,
- 699 Tjiputra, J., Toyama, K., Tsujino, H., Watanabe, M., Yamamoto, A., Yool, A., and Ziehn, T.:
- 700 Twenty-first century ocean warming, acidification, deoxygenation, and upper-ocean nutrient and
- primary production decline from CMIP6 model projections, Biogeosciences, 17, 3439–3470,
- 702 https://doi.org/10.5194/bg-17-3439-2020, 2020.
- Mahowald, N. M., Muhs, D. R., Levis, S., Rasch, P. J., Yoshioka, M., Zender, C. S., and Luo, C.:
- 704 Change in atmospheric mineral aerosols in response to climate: Last glacial period, preindustrial,
- modern, and doubled carbon dioxide climates: DUST RESPONSE TO CLIMATE, J. Geophys.
- Res. Atmospheres, 111, n/a-n/a, https://doi.org/10.1029/2005JD006653, 2006.
- 707 McMahon, P. B. and Chapelle, F. H.: Microbial production of organic acids in aquitard
- sediments and its role in aquifer geochemistry, Nature, 349, 233–235,
- 709 https://doi.org/10.1038/349233a0, 1991.
- 710 Middelburg, J. J. and Levin, L. A.: Coastal hypoxia and sediment biogeochemistry,
- 711 Biogeosciences, 6, 1273–1293, https://doi.org/10.5194/bg-6-1273-2009, 2009a.

- 712 Middelburg, J. J. and Levin, L. A.: Coastal hypoxia and sediment biogeochemistry, 1273–1293,
- 713 2009b.
- Mills, M. M., Ridame, C., Davey, M., La Roche, J., and Geider, R. J.: Iron and phosphorus co-
- 715 limit nitrogen fixation in the eastern tropical North Atlantic, Nature, 429, 292–294,
- 716 https://doi.org/10.1038/nature02550, 2004.
- Moore, J. K. and Braucher, O.: Sedimentary and mineral dust sources of dissolved iron to the
- vorld ocean, Biogeosciences, 5, 631–656, https://doi.org/10.5194/bg-5-631, 2008.
- Moore, J. K., Doney, S. C., Kleypas, J. A., Glover, D. M., and Fung, I. Y.: An intermediate
- 720 complexity marine ecosystem model for the global domain, Deep Sea Res. Part II Top. Stud.
- 721 Oceanogr., 49, 403–462, https://doi.org/10.1016/S0967-0645(01)00108-4, 2001.
- Moore, J. K., Doney, S. C., and Lindsay, K.: Upper ocean ecosystem dynamics and iron cycling
- in a global three-dimensional model: GLOBAL ECOSYSTEM-BIOGEOCHEMICAL MODEL,
- 724 Glob. Biogeochem. Cycles, 18, n/a-n/a, https://doi.org/10.1029/2004GB002220, 2004.
- Noffke, A., Hensen, C., Sommer, S., Scholz, F., Bohlen, L., Mosch, T., Graco, M., and
- Wallmann, K.: Benthic iron and phosphorus fluxes across the Peruvian oxygen minimum zone,
- 727 Limnol. Oceanogr., 57, 851–867, https://doi.org/10.4319/lo.2012.57.3.0851, 2012.
- 728 Pham, A. L. D. and Ito, T.: Formation and Maintenance of the GEOTRACES Subsurface-
- 729 Dissolved Iron Maxima in an Ocean Biogeochemistry Model, Glob. Biogeochem. Cycles, 32,
- 730 932–953, https://doi.org/10.1029/2017GB005852, 2018.
- Pham, A. L. D. and Ito, T.: Ligand Binding Strength Explains the Distribution of Iron in the
- North Atlantic Ocean, Geophys. Res. Lett., 46, 7500–7508,
- 733 https://doi.org/10.1029/2019GL083319, 2019.
- Pozo Buil, M. and Di Lorenzo, E.: Decadal dynamics and predictability of oxygen and
- subsurface tracers in the California Current System, Geophys. Res. Lett., 44, 4204–4213,
- 736 https://doi.org/10.1002/2017GL072931, 2017.
- Qin, Q., Kinnaman, F. S., Gosselin, K. M., Liu, N., Treude, T., and Valentine, D. L.: Seasonality
- of water column methane oxidation and deoxygenation in a dynamic marine environment,
- 739 Geochim. Cosmochim. Acta, 336, 219–230, https://doi.org/10.1016/j.gca.2022.09.017, 2022.
- Reimers, C. E., Lange, C. B., Tabak, M., and Bernhard, J. M.: Seasonal spillover and varve
- 741 formation in the Santa Barbara Basin, California, Limnol. Oceanogr., 35, 1577–1585,
- 742 https://doi.org/10.4319/lo.1990.35.7.1577, 1990.
- Renault, L., Deutsch, C., McWilliams, J. C., Frenzel, H., Liang, J.-H., and Colas, F.: Partial
- decoupling of primary productivity from upwelling in the California Current system, Nat.
- 745 Geosci., 9, 505–508, https://doi.org/10.1038/ngeo2722, 2016.

- Renault, L., McWilliams, J. C., Kessouri, F., Jousse, A., Frenzel, H., Chen, R., and Deutsch, C.:
- 747 Evaluation of high-resolution atmospheric and oceanic simulations of the California Current
- 748 System, Prog. Oceanogr., 195, 102564, https://doi.org/10.1016/j.pocean.2021.102564, 2021.
- Sañudo-Wilhelmy, S., Kustka, A., Gobler, C., Hutchins, D., Yang, M., Lwiza, K., Burns, J.,
- Raven, J., and Carpenter, E.: Phosphorus limitation of nitrogen fixation by Trichodesmium in the
- 751 central Atlantic Ocean, Nature, 411, 66–9, https://doi.org/10.1038/35075041, 2001.
- 752 Severmann, S., McManus, J., Berelson, W. M., and Hammond, D. E.: The continental shelf
- benthic iron flux and its isotope composition, Geochim. Cosmochim. Acta, 74, 3984–4004,
- 754 https://doi.org/10.1016/j.gca.2010.04.022, 2010.
- 755 Shchepetkin, A. F.: An adaptive, Courant-number-dependent implicit scheme for vertical
- advection in oceanic modeling, Ocean Model., 91, 38–69,
- 757 https://doi.org/10.1016/j.ocemod.2015.03.006, 2015.
- 758 Shchepetkin, A. F. and McWilliams, J. C.: The regional oceanic modeling system (ROMS): a
- split-explicit, free-surface, topography-following-coordinate oceanic model, Ocean Model., 9,
- 760 347–404, https://doi.org/10.1016/j.ocemod.2004.08.002, 2005.
- Shiller, A. M., Gieskes, J. M., and Brian Price, N.: Particulate iron and manganese in the Santa
- 762 Barbara Basin, California, Geochim. Cosmochim. Acta, 49, 1239–1249,
- 763 https://doi.org/10.1016/0016-7037(85)90013-4, 1985.
- 764 Sholkovitz, E. and Soutar, A.: Changes in the composition of the bottom water of the Santa
- Barbara Basin: effect of turbidity currents, Deep Sea Res. Oceanogr. Abstr., 22, 13–21,
- 766 https://doi.org/10.1016/0011-7471(75)90014-5, 1975.
- 767 Sholkovitz, E. R. and Gieskes, J. M.: A PHYSICAL-CHEMICAL STUDY OF THE FLUSHING
- 768 OF THE SANTA BARBARA BASIN1: FLUSHING OF THE SANTA BARBARA BASIN,
- 769 Limnol. Oceanogr., 16, 479–489, https://doi.org/10.4319/lo.1971.16.3.0479, 1971.
- Sigman, D. M., Robinson, R., Knapp, A. N., van Geen, A., McCorkle, D. C., Brandes, J. A., and
- 771 Thunell, R. C.: Distinguishing between water column and sedimentary denitrification in the
- Santa Barbara Basin using the stable isotopes of nitrate, Geochem. Geophys. Geosystems, 4,
- 773 https://doi.org/10.1029/2002GC000384, 2003.
- Soetaert, K., Middelburg, J. J., Herman, P. M. J., and Buis, K.: On the coupling of benthic and
- pelagic biogeochemical models, Earth-Sci. Rev., 51, 173–201, https://doi.org/10.1016/S0012-
- 776 8252(00)00004-0, 2000.
- Sommer, S., Gier, J., Treude, T., Lomnitz, U., Dengler, M., Cardich, J., and Dale, A. W.:
- 778 Depletion of oxygen, nitrate and nitrite in the Peruvian oxygen minimum zone cause an
- imbalance of benthic nitrogen fluxes, Deep Sea Res. Part Oceanogr. Res. Pap., 112, 113–122,
- 780 https://doi.org/10.1016/j.dsr.2016.03.001, 2016.

- Tagliabue, A., Sallée, J.-B., Bowie, A. R., Lévy, M., Swart, S., and Boyd, P. W.: Surface-water
- iron supplies in the Southern Ocean sustained by deep winter mixing, Nat. Geosci., 7, 314–320,
- 783 https://doi.org/10.1038/ngeo2101, 2014.
- Tagliabue, A., Aumont, O., DeAth, R., Dunne, J. P., Dutkiewicz, S., Galbraith, E., Misumi, K.,
- Moore, J. K., Ridgwell, A., Sherman, E., Stock, C., Vichi, M., Völker, C., and Yool, A.: How
- 786 well do global ocean biogeochemistry models simulate dissolved iron distributions?: GLOBAL
- 787 IRON MODELS, Glob. Biogeochem. Cycles, 30, 149–174,
- 788 https://doi.org/10.1002/2015GB005289, 2016.
- Tagliabue, A., Bowie, A. R., Boyd, P. W., Buck, K. N., Johnson, K. S., and Saito, M. A.: The
- 790 integral role of iron in ocean biogeochemistry, Nature, 543, 51–59,
- 791 https://doi.org/10.1038/nature21058, 2017.
- 792 Testa, J. M., Brady, D. C., Di Toro, D. M., Boynton, W. R., Cornwell, J. C., and Kemp, W. M.:
- 793 Sediment flux modeling: Simulating nitrogen, phosphorus, and silica cycles, Estuar. Coast. Shelf
- 794 Sci., 131, 245–263, https://doi.org/10.1016/j.ecss.2013.06.014, 2013.
- 795 Till, C. P., Solomon, J. R., Cohen, N. R., Lampe, R. H., Marchetti, A., Coale, T. H., and Bruland,
- 796 K. W.: The iron limitation mosaic in the California Current System: Factors governing Fe
- availability in the shelf/near-shelf region, Limnol. Oceanogr., 64, 109–123,
- 798 https://doi.org/10.1002/lno.11022, 2019.
- 799 Treude, T., Smith, C. R., Wenzhöfer, F., Carney, E., Bernardino, A. F., Hannides, A. K., Krüger,
- 800 M., and Boetius, A.: Biogeochemistry of a deep-sea whale fall: sulfate reduction, sulfide efflux
- and methanogenesis, Mar. Ecol. Prog. Ser., 382, 1–21, 2009.
- Valentine, D. L., Fisher, G. B., Pizarro, O., Kaiser, C. L., Yoerger, D., Breier, J. A., and Tarn, J.:
- 803 Autonomous Marine Robotic Technology Reveals an Expansive Benthic Bacterial Community
- Relevant to Regional Nitrogen Biogeochemistry, Environ. Sci. Technol., 50, 11057–11065,
- 805 https://doi.org/10.1021/acs.est.6b03584, 2016.
- Wallmann, K., José, Y. S., Hopwood, M. J., Somes, C. J., Dale, A. W., Scholz, F., Achterberg,
- 807 E. P., and Oschlies, A.: Biogeochemical feedbacks may amplify ongoing and future ocean
- deoxygenation: a case study from the Peruvian oxygen minimum zone, Biogeochemistry, 159,
- 809 45–67, https://doi.org/10.1007/s10533-022-00908-w, 2022.
- White, M. E., Rafter, P. A., Stephens, B. M., Wankel, S. D., and Aluwihare, L. I.: Recent
- 811 Increases in Water Column Denitrification in the Seasonally Suboxic Bottom Waters of the
- Santa Barbara Basin, Geophys. Res. Lett., 46, 6786–6795,
- 813 https://doi.org/10.1029/2019GL082075, 2019.
- Widdows, J. and Brinsley, M.: Impact of biotic and abiotic processes on sediment dynamics and
- the consequences to the structure and functioning of the intertidal zone, J. Sea Res., 48, 143–156,
- 816 https://doi.org/10.1016/S1385-1101(02)00148-X, 2002.

- Yao, M., Henny, C., and Maresca, J. A.: Freshwater Bacteria Release Methane as a By-Product
- of Phosphorus Acquisition, Appl. Environ. Microbiol., 82, 6994–7003,
- 819 https://doi.org/10.1128/AEM.02399-16, 2016.
- Yousavich, D. J., Robinson, D., Peng, X., Krause, S. J. E., Wenzhoefer, F., Janßen, F., Liu, N.,
- 821 Tarn, J., Kinnaman, F., Valentine, D. L., and Treude, T.: Marine anoxia initiates giant sulfur-
- bacteria mat proliferation and associated changes in benthic nitrogen, sulfur, and iron cycling in
- 823 the Santa Barbara Basin, California Borderland, EGUsphere, 1–48,
- 824 https://doi.org/10.5194/egusphere-2023-1198, 2023.

- 825 Zhou, Y., Gong, H., and Zhou, F.: Responses of Horizontally Expanding Oceanic Oxygen
- 826 Minimum Zones to Climate Change Based on Observations, Geophys. Res. Lett., 49,
- 827 e2022GL097724, https://doi.org/10.1029/2022GL097724, 2022.